

MASS SPECTROMETER STUDY OF LASER PLASMA

Yu. A. BYKOVSKIĬ, N. N. DEGTYARENKO, V. F. ELESIN, Yu. P. KOZYREV, and S. M. SIL'NOV

Moscow Engineering Physics Institute

Submitted July 14, 1970; resubmitted November 16, 1970

Zh. Eksp. Teor. Fiz. 60, 1306–1319 (April, 1971)

A mass spectrometer was used to investigate the interaction between a high-intensity laser beam and a solid target. The yield of multiply-charged ions, and their energy and angular distributions have been determined. The degree of ionization has been measured as a function of the laser intensity, and the ion energies have been determined. An analysis of the energy distributions is reported and the effect of recombination on these distributions is evaluated.

THE interaction between laser radiation and various materials has been attracting considerable attention. It is well known^[1-4] that laser radiation of intensity $q \gtrsim 10^8 \text{ W/cm}^2$ will produce a plasma bunch of high temperature and density on the surface of an opaque solid target and this will absorb a large proportion of the light energy. The time-of-flight mass spectrometer^[5-9] is particularly convenient for the investigation of this type of laser plasma.

In this paper we discuss in detail the formation of multiply-charged ions, and their energy and angular distributions for intensities in the range $10^8 - 10^{13} \text{ W-cm}^{-2}$.

The basic elements of the experimental setup were a laser, a time-of-flight analyzer, a mass spectrometer, an ion detector, and an electron multiplier connected to a double-beam oscillograph. A detailed description of the recording part of the apparatus is given in^[6].

The laser part of the setup consisted of a generator and two neodymium amplifiers. For low q , only the generator was employed. The maximum generated laser power per pulse was $W \sim 2 \text{ GW}$ which for a linear size of the focal spot amounting to $d \sim 0.01 - 0.1 \text{ cm}$ ensured an intensity of up to $q \sim 10^{13} \text{ W-cm}^{-2}$.

Q switching was produced by a chemical shutter incorporating a solution of vanadium phthalocyanine in nitrobenzene. The laser pulse length was $\tau \sim 40 \text{ nsec}$ which was reduced to $\tau \sim 15 \text{ nsec}$ after passing through the amplifiers. Beam focusing on the surface of the target, located in the ion source, was produced by a lens with a focal length $f = 5 \text{ cm}$. The working vacuum was maintained at 10^{-6} torr , and the ion flight distance between the target and the detector was 450 cm . The ion mass resolution of the system was $M/\Delta M \sim 100$.

1. EXPERIMENTAL RESULTS

Our method of investigating laser plasma enables us to obtain extensive data on ions emitted by the target, including the number of charges per plasma ion, the energy distribution of ions of given charge and mass for different laser parameters, and the ion angular distribution.

Yield of Multiply-charged Ions

When the various components of spreading plasma are recorded on the oscillograph screen, ions of differ-

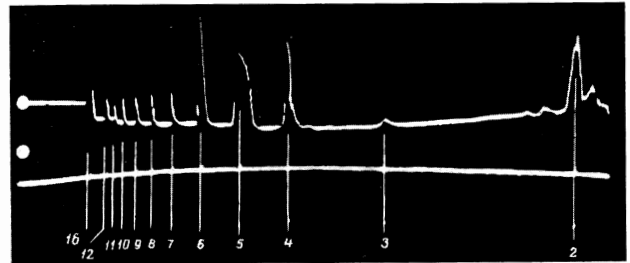


FIG. 1. Oscillograms showing ion currents for Co_{59}^{27} (numbers show the ion charge).

ent charge appear in the form of peaks, each of which corresponds to an ion-current pulse from the detector. For example, Fig. 1 shows the ion-current oscillogram for Co_{59}^{27} . For a particular magnet current in the mass spectrometer and a particular time base, the peaks correspond to cobalt ions with charge numbers between $z = 2$ and $z = 16$. Experiments have shown that, at sufficiently low laser intensities $q \sim 10^8 \text{ W-cm}^{-2}$, it is possible to produce plasma bunches consisting exclusively of ions with $z = 1$ on targets of different elements.

As the laser intensity increases, one detects ions with higher z , and the number of such ions continuously increases. Ions with charges up to $z = 25$ ^[8] have been obtained with Co_{59}^{27} using $q \sim 10^{13} \text{ W-cm}^{-2}$.

The number of recorded ions with different z is different for different materials. Figure 2 shows the number of ions as a function of their charge for three materials, namely, Ta_{181}^{73} , W_{184}^{74} , and Co_{59}^{27} , recorded within solid angles between $\sim 10^{-7}$ and $\sim 10^{-8}$. The intensity in these experiments was $10^{13} \text{ W-cm}^{-2}$. The maximum number of ions in the case of cobalt for $z = 1 - 2$ was about $10^6 - 10^7$. The number of ions decreases monotonically with increasing z . Thus, the number of cobalt ions with z in excess of 20 is about 1000 under these experimental conditions.

Ion Energy Spectrum

Measurements of the energy spectra have shown that the mean energy of the recorded ions is well in excess of their thermal energy in the plasma during the incidence of the laser pulse. This shows that the ions are accelerated as the plasma bunch spreads out.

Figure 3 shows the energy distribution of Al_{27}^{13} ions

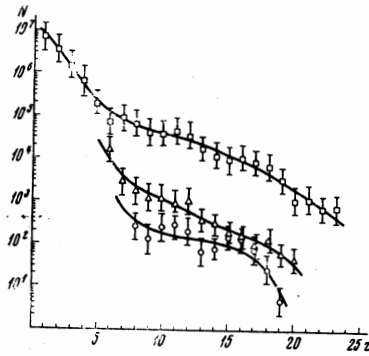


FIG. 2. Number of ions as a function of charge for $q \sim 10^{13} \text{ W-cm}^{-2}$. \square —Co₅₉²⁷, Δ —Ta₁₈₁⁷³, \circ —W₁₈₄⁷⁴.

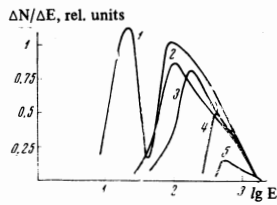


FIG. 3. Energy distribution of Al₂₇¹³ ions (numbers 1-5 represent number of charges).

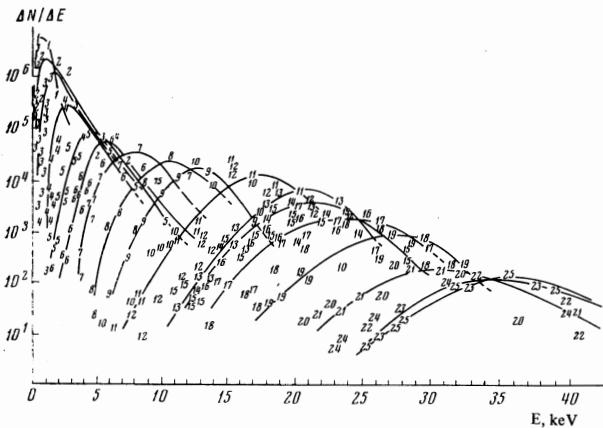


FIG. 4. Energy distribution of Co₅₉²⁷ ions (numbers 1-25 represent the number of charges per ion; for $z \geq 10$ the curves are given only for odd z).

with z up to 5 for laser intensities $q \sim 8 \times 10^9 \text{ W-cm}^{-2}$. The curve corresponding to singly charged ions shows two peaks. The first peak is observed at an ion energy of about 20 eV ("thermal" ions) and the second at 100 eV ("accelerated" ions).

The energy distributions were also obtained for Co, Ta, and W targets at much higher laser intensities. Figure 4 shows the energy distributions for Co ions up with z up to 25, produced during the incidence of a single laser pulse of intensity $\sim 10^{13} \text{ W-cm}^{-2}$. For the same value of q , the overall shape of the distributions for Ta and W ions is the same, but the maximum value of z is lower, i.e., -20 for Ta and $+19$ for W.

The energy distributions show substantial energy spreads. The maximum energy values are observed for the highest values of z and reach 30–40 keV. Since all the distributions occupy an unusually large energy interval, and are highly non-Maxwellian, it is natural to suppose that the temperature distribution over the

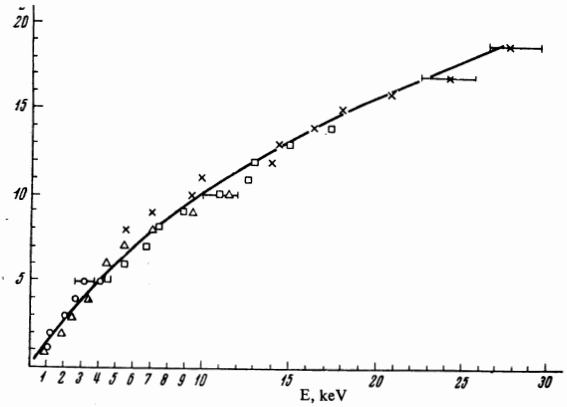


FIG. 5. Energy of W₁₈₄⁷⁴ ions as a function of charge per ion for different values of q : \circ — $q \approx 10^9 \text{ W-cm}^{-2}$; Δ — $2 \times 10^{12} \text{ W-cm}^{-2}$, \square — $5 \times 10^{12} \text{ W-cm}^{-2}$, \times — $10^{13} \text{ W-cm}^{-2}$.

plasma-flare surface is highly inhomogeneous either in time or in space.

An important feature of the spectra is the position of the peaks on the multiply-charged ion distributions. It is clear from Fig. 4 that, as z increases, the distribution peaks for the corresponding ions shift toward higher energies.

By analyzing the energy distribution data we have obtained the ion energies as functions of ion charge. The corresponding curve for tungsten is shown in Fig. 5. The shape of the curve for the other elements is quite similar.

The energy distributions change their shape as the laser intensity is varied. Experiments show (Fig. 5) that the first effect to appear is a change in the maximum charge of the recorded ions. As the intensity increases, the energy distribution broadens in the direction of higher energies, mainly due to the appearance of ions with high z which have higher energies. The energy of ions recorded at lower q , on the other hand, is not very dependent on the radiation intensity.

We have performed a series of measurements of the energy distributions for Mn₅₅²⁵ at intensities corresponding to threshold values for the formation of low- z ions.

Figure 6 shows the results of these measurements. The radiation intensity was varied with the aid of a filter. The experimental uncertainties prevented us, in some cases, from obtaining unambiguous ion-energy distribution curves, but there is a clear overall tendency in the formation of the spectra.

Figure 6a ($q \sim 2.5 \times 10^8 \text{ W-cm}^{-2}$) shows that there are only ions with $z = 1$, and these occupy the energy range ~ 25 –75 eV. The distribution peak is shifted toward lower energies at about 40 eV. For the next value of intensity ($q \sim 4.3 \times 10^8 \text{ W-cm}^{-2}$) we observed ions with $z = 2$ in the energy interval 100–200 eV. At the same time, the singly-charged ion distribution shows a second peak in roughly the same energy range.

When q is increased up to 5.5×10^8 and 10^9 W-cm^{-2} there is an increase in the energy range in which ions with $z = 1$ and $z = 2$ are recorded, and there is an obvious correlation between the appearance of the third peak on the singly-charged ion distribution and the second peak on the doubly-charged ion distribution. There is a clear relation between the energy intervals

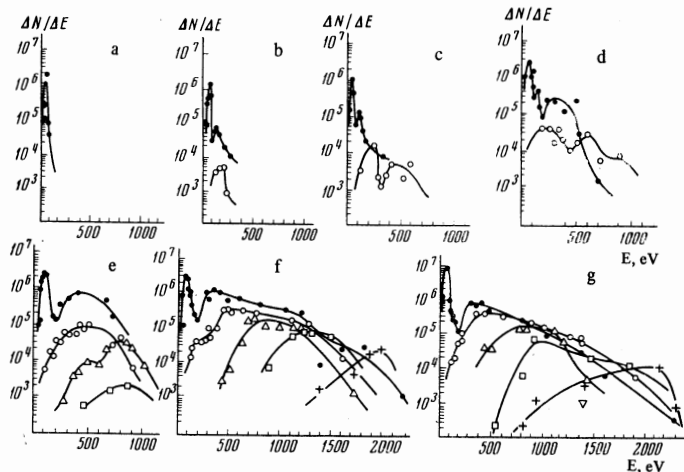


FIG. 6. Energy spectra of Mn_{25}^{25} ions for different laser intensities q ($W\text{-cm}^{-2}$): a— $q \approx 2.5 \times 10^8$, b— 4.3×10^8 , c— 5.5×10^8 , d— 10^9 , e— 2.5×10^9 , f— 8.5×10^9 , g— 10^{10} , charge per ion: \circ — $z = 1$, \square — 2 , Δ — 3 , \square — 4 , ∇ — 5 , ∇ — 6 .

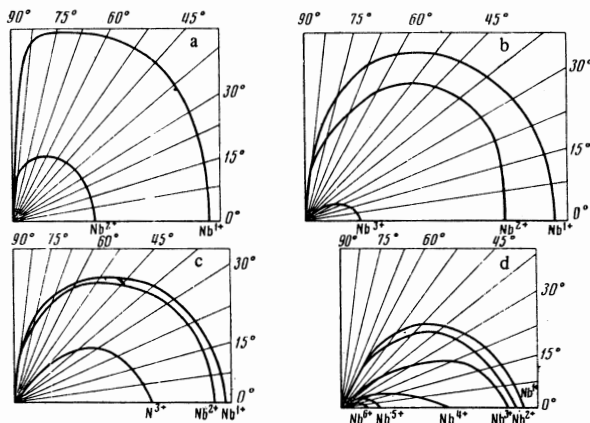


FIG. 7. Angular distribution of ions of different energies (Nb_{93}^{41}): a— $E = 100$ eV, b—400 eV, c—600 eV, d—1000 eV.

occupied by the two peaks and their correlated growth with increasing intensity.

When $q \sim 10^9$ $W\text{-cm}^{-2}$ there is a third peak on the doubly-charged ion distribution.

It is clear from Figs. 6c and d that the first and second peaks on the singly-charged ion curve gradually begin to combine and eventually form a single peak at $q \sim 2.5 \times 10^9$ $W\text{-cm}^{-2}$. The same tendency is shown by ion distributions corresponding to all other values of z as the intensity increases.

Angular Distribution of the Ions

The angular distribution of the emitted material under the action of a giant laser pulse was investigated in^[10]. In the present work we measured the angular distribution of ions with different charge z . The target was mounted in a special rotatable holder so that we were able to direct ions emitted at different angles to the target normal into the analyzing system. The angular distributions were calculated from the energy distributions at a number of fixed angles.

Figure 7 shows the angular distributions for Nb_{93}^{41} ions with charges up to $z = 6$ at ion energies of 100, 400,

600, and 1000 eV. As the charge z and the ion energy increase, the angular distributions lie closer to the normal. This type of effect is observed independently of the angle of incidence of the laser beam.

Individual bursts were noted during the angular distribution measurements, but these are smoothed out in Fig. 7 since reliable determination of the fine structure of the ion angular distributions will require more accurate measurements.

2. DISCUSSION

In this section we shall analyze the experimental data with a view to estimating the degree of ionization and the energy of multiply-charged ions, as well as the mechanism responsible for the shape of the energy spectra.

The gas-dynamic phenomena connected with heating and the re-emission of absorbed material have been discussed theoretically in^[2,3]. It was shown that, in the case of plane, one-dimensional, gas-dynamic motion, there is a self-consistent state,^[2] whereas in the case of spherical emission of material and the associated transparency of peripheral regions of the plasma there is a time-independent state.^[3] The latter corresponds to a more realistic formulation of the problem of plasma heating by a focused laser beam, and is determined by the condition $l(\rho, T) \sim d$, where l is the laser photon mean free path in the plasma, and d is the linear size of the focal spot on the target (under our conditions $d < 7 \times 10^{-2}$ cm). The estimated time t_1 after which the self-consistent state goes over into the state governed by the spherical nature of the motion is estimated in^[3,4]. Calculations of t_1 for our experimental conditions show that the time-independent state is reached during the laser pulse length τ .

Multiple ionization processes must be taken into account when the laser radiation is incident on a heavy-atom target. Energy losses by the ionization of atoms are usually neglected, which is valid for light atoms and the formation of fully ionized plasma (hydrogen plasma). For heavy-atom plasmas these losses must be taken into account and, moreover, in this case, the degree of ionization z of the atoms, the temperature T , and the plasma density ρ are not independent.

The interpretation put forward below explains satisfactorily the experimental results and is based on the assumed thermodynamic equilibrium in the plasma, and the achievement of a time-independent evaporation process and the heating of the material during the incidence of the laser pulse.^[3,4] Under the conditions of thermodynamic equilibrium, the distribution of the ions over the degree of ionization z should have a relatively narrow peak with a width of $\Delta z \sim 2-3$, i.e. the plasma contains mostly ions with charge numbers 2 or 3.^[11] When the laser pulse was incident on the target we recorded ions with z between 1 and z_{\max} .

It is assumed that the appearance of this set of ions is due to the space and time variation in the intensity of the radiation incident on the target. In the time-independent state, T and ρ and, consequently, z as well, are determined by the instantaneous power $W(t)$ and the size d of the focal spot, but these parameters undergo a substantial change during the laser pulse time τ . Conse-

quently, the plasma temperature and density under these conditions must vary during the pulse, and this leads to the emission of ions with charges between $z = 1$ and z_{\max} which corresponds to the maximum incident laser intensity.

Analysis of the experimental data shows that groups of ions with the corresponding T and z are emitted independently. It is assumed that the maximum ion velocity can be found from the condition for time-independent adiabatic emission of the ultrasonic part of the plasma flare. If this is so, it is a simple matter to take into account the work done by the electron gas in accelerating the ions (the electrons, which are much faster, tend to be emitted first, and the associated electric field which maintains the quasi-neutrality of the plasma accelerates ions up to the electron velocities^[12]). The effect of recombinational heating on the spreading of plasma is quite simply taken into account in this formulation of the problem.

Estimated Degree of Ionization

In the thermodynamic approximation^[11] we have

$$\frac{I(z)}{T} = \ln \frac{AT^{n/2}}{zn}, \quad (1)$$

where $I(z)$ is the ionization potential for the z -th electron, n is the density of the atoms, and $A = 6 \times 10^{21} \text{ eV}^{-3/2} \text{ cm}^{-3}$.

The internal energy of the multiply ionized plasma in this case is given by

$$\varepsilon = \frac{3}{2} NkT(1+z) + NQ, \quad Q = \sum_z I(z), \quad (2)$$

where N is the number of atoms per gram.

This expression can be transformed if we recall that $p = kT(1+z)n$:

$$\varepsilon = \frac{p}{\rho} \left[\frac{3}{2} + \frac{Q(z)}{(1+z)kT} \right]. \quad (3)$$

The equation for a gas with constant specific heat ($\gamma = \text{const}$) is

$$\varepsilon = \frac{p}{\rho} \frac{1}{(\gamma-1)}.$$

The multiply ionized plasma can be described by analogy by introducing an effective γ' defined by

$$(\gamma' - 1)^{-1} = \frac{3}{2} + \frac{Q(z)}{(1+z)kT}. \quad (4)$$

It turns out that, for a broad range of values of z , the quantity γ' is a slowly varying function, lying between 1.2 and 1.3, since for $z > 1$ we have $I/kT \sim \text{const} \sim 10$.^[11] We shall henceforth neglect the change in the quantity $\sim \gamma'$ and retain only $(\gamma' - 1)^{-1}$.

Using Eq. (4), we can transform Eq. (2) so that it reads

$$\varepsilon = NkT[1 + z(T; \rho)](\gamma' - 1)^{-1}. \quad (5)$$

Let us now express the internal energy of the plasma in terms of the laser-pulse parameters. The main process in the absorption of photons with energy $\hbar\omega \sim 1 \text{ eV}$ by the plasma is governed by free-free transitions of electrons in the field of the ions. Bound-free absorption will be neglected because its contribution to

the overall plasma absorption coefficient, which is determined by the ratio $\hbar\omega/kT$ ^[11] is small ($kT > \hbar\omega \sim 1-2 \text{ eV}$).

The absorption coefficient K of the plasma depends on the plasma state parameters z , T , and ρ . In the case of absorption due to free-free transitions we have, taking stimulated emission into account,

$$K \sim z^2 \rho^2 T^{-3/2}.$$

We shall now need an expression for the absorption coefficient of multiply-ionized plasma as a function of density and internal energy. We have from Eq. (5)

$$K = \kappa_1(\varepsilon; \rho) \rho^2 \varepsilon^{-3/2}, \quad (6)$$

where

$$\kappa_1(\varepsilon; \rho) \approx 5 \cdot 10^{28} z^2 (1+z)^{3/2} (\gamma' - 1)^{-3/2} \quad (7)$$

depends on the temperature and density of the plasma through z and $(\gamma' - 1)$. Thus, the heating and outflow of the laser plasma produced on a target with a high atomic weight μ , i.e., with $z = z(T, \rho)$, can be described by taking into account only the multiple ionization processes and their effect on the absorption of radiation.

Under the conditions of time-independent evaporation and heating of the target material, the ionized state which is described by the equation with γ' can, by analogy with^[3,4], be used to find the following expressions for the internal energy ε and density ρ of the plasma:

$$\begin{aligned} \varepsilon &\approx \alpha_1 W^{1/2} \kappa_1^{3/2} d^{-3/2} (\gamma' - 1)^{-3/2}, \\ \rho &\approx \alpha_2 W^{1/2} \kappa_1^{-1/2} d^{-1} (\gamma' - 1)^{-1/2}, \end{aligned} \quad (8)$$

where W is the laser radiation power, and α_1 and α_2 are constants.

Using Eqs. (5) and (7), we obtain the following expressions for the temperature and density of the atoms:

$$\begin{aligned} T &= \frac{z^{3/2}}{(1+z)^{3/2}} (\gamma' - 1)^{3/2} W^{1/2} d^{-3/2} \beta_1, \\ n &= \frac{1}{z(1+z)^{1/2}} (\gamma' - 1)^{1/2} W^{1/2} d^{-1} \beta_2, \end{aligned} \quad (9)$$

where

$$\begin{aligned} \beta_1 &\approx 0.32 \mu^{3/2} [\text{eV} \cdot \text{cm}^{2/3} \text{MW}^{-4/3}], \\ \beta_2 &\approx 2.6 \cdot 10^{18} \mu^{1/2} [\text{cm}^{-2} \text{MW}^{-1/3}]. \end{aligned}$$

Substituting Eq. (9) into Eqs. (1) and (4), we obtain the following transcendental equation for z and $\gamma' - 1$:

$$\begin{aligned} I(z) &\approx \beta_1 \frac{W^{1/2} (\gamma' - 1)^{1/2}}{d^{3/2}} \ln [\beta_2 z^{1/2} (\gamma' - 1)^{1/2} W^{1/2}] \\ (\gamma' - 1)^{-1} &\approx \frac{3}{2} + \frac{Q(z)}{1+z} \frac{d^{3/2}}{\beta_1 (\gamma' - 1)^{1/2} W^{1/2}} \end{aligned} \quad (10)$$

where

$$\beta_3 \approx 5.6 \cdot 10^8 \mu^{1/2} [\text{MW}^{-1/3}].$$

The above equations cannot be solved unless we know the ionization potentials of the material on which the laser radiation is incident. Since the $I(z)$ have been determined for only a few values of z , the ionization potentials were calculated from the approximate formula^[13]

$$I_m(z) = I_n(1) + [I_{n+1}(2) - I_n(1)](z-1) + k_n(z-1)(z-2), \quad (11)$$

where m and n are the position numbers of the elements, $n = (m+1) - z$, and k_n is a numerical factor.

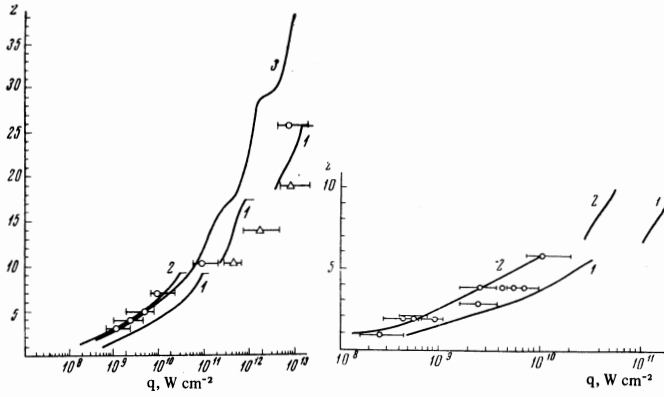


FIG. 8

FIG. 9

FIG. 8. Number of charges per ion, z , as a function of laser radiation intensity q : 1—Co₅₉²⁷ ($d_1 \sim 10^{-2}$ cm); 2—Co₅₉²⁷ ($d_2 \sim 10^{-1}$ cm); 3—Ta₁₈₁⁷³ and W₁₈₄⁷⁴ ($d \sim 10^{-2}$ cm). Experimental values of z correspond to O—Co₅₉²⁷, Δ —Ta₁₈₁⁷³ and W₁₈₄⁷⁴.

FIG. 9. Number of charges per ion as a function of laser intensity q for Mn₅₅²⁵ (1— $d \sim 10^{-2}$ cm, 2— $d \sim 10^{-1}$ cm). Experimental values of z correspond to $d \sim 10^{-1}$ cm.

The table for k_n , given in^[13], contains no data for $n = 19-28$ and $37-45$, which correspond to the ionization of the d and f electron shells of atoms. For these values of n we cannot use Eq. (11) and we must employ a linear approximation to find the ionization potentials. The above method was used to calculate the ionization potentials $I(z)$ and values of the function $Q(z)$ for different elements.

The numerical solution of Eq. (10) was used to construct theoretical curves for the degree of ionization of Co, Mn, Ta, and W atoms for different incident laser intensities q , and two values of the focal spot diameter (Figs. 8 and 9). The results for Ta₁₈₁⁷³ and W₁₈₄⁷⁴ are very similar and are combined in a single curve. The plateaus on the curves are connected with transitions to the ionization of new electron shells. Figures 8 and 9 indicate the experimental values of q for which ions with given z are found to appear. The experimental points for $q \leq 10^{10}$ W-cm⁻² correspond to a linear focal-spot size $d \sim 0.1$ cm. Good agreement between experimental and theoretical values can be seen to occur for cobalt and manganese. For Ta and W the experiments were performed only for high q and $d \sim 0.01$ cm, and ions with lower z were observed than would be expected on the basis of Eq. (10) for intensities of $10^{12}-10^{13}$ W-cm⁻².

We assumed that the discrepancy was due to the more intensive recombination of heavy-element ions. This agrees with the dependence of the number of ions on z shown in Fig. 2 (compare this with Co and Ta, W). However, this discrepancy could also be due to the absence of ionization equilibrium for these elements at high q .^[14]

Estimated Energy of Multiply-charged Ions

Analysis of the measured ion energies for given z as functions of the incident intensity (Fig. 5) enables us to assume that ions with given temperature T and charge z are emitted independently. In fact, when q changes by four order of magnitude the ion energy changes by a factor of not more than two.

The maximum ion velocity can be estimated from the condition for the adiabatic emission of the ultrasonic part of the plasma flare

$$\epsilon_1 + \frac{p_1}{\rho_1} + \frac{v_1^2}{2} = \epsilon_\infty + \frac{v_\infty^2}{2}. \quad (12)$$

The left-hand side of this equation refers to the acoustic cross section ($v_1 = c = \sqrt{(\gamma' - 1)\gamma'\epsilon}$), in which the plasma parameters are determined by Eq. (10). Here, $\epsilon_\infty = NQ(z_\infty)$ is the internal energy of the plasma after emission, and z_∞ is the effective degree of ionization after the emission of the plasma.

The assumed adiabatic nature of the process is justified by the weak absorption of laser radiation in the ultrasonic part of the flare due to the strong reduction in density.^[3]

We shall use Eq. (12) to calculate the ion energy in the following two limiting cases:

1. The ionization energy almost completely transformed into thermal energy and then into hydrodynamic energy, i.e., recombinational heating is important. Since under these conditions $\epsilon_\infty \ll v_\infty^2/2$, we have the following formula from Eq. (12) for the velocity of emission in terms of the plasma parameters in the acoustic cross section:

$$v_\infty^2 = \frac{\gamma' + 1}{\gamma' - 1} c^2.$$

2. In the opposite limiting case, when recombinational heating is small, we have

$$\epsilon_{\infty 2} = N \sum_{z_1}^{\infty} I(z) \approx N \sum_{z_1}^{z_1} I(z) \approx \left(\frac{5}{2} - \frac{3}{2} \gamma' \right) \epsilon_1,$$

where z_1 is the absorption multiplicity in the acoustic cross section. In this case, the emission velocity is $v_{\infty 2}^2 = (\gamma' + 5)c^2/\gamma'$, and the ion kinetic energy is given by

$$E_1 = \frac{\gamma' + 1}{\gamma' - 1} \frac{\gamma'}{2} kT(1 + z), \quad (13a)$$

$$E_2 = \frac{\gamma' + 5}{2} kT(1 + z). \quad (13b)$$

The last formulas were used to calculate the ion energy as a function of their charge for Co and Mn (Figs. 10, 11).

The order of magnitude of the energy in the case of Co and high values of z agrees with experimental data (Fig. 10). Since the experimental energy for $z \sim 20$ lies between E_1 and E_2 , it may be supposed that for highly charged ions with much higher emission velocity the recombinational heating processes are less important than for slower ions with lower z . It follows that for multiply charged ions the ionization "quenching" process^[11] begins much more rapidly, and the energy spectrum of the ions is determined only by the conditions of their formation and emission.

For ions with $z \lesssim 10$ the energies calculated with allowance for complete recombinational heating are less than the minimum recorded energy of these ions (Fig. 11). A shift of the theoretical curve by one or two units toward lower z gives good agreement with the experimental points, and this confirms that recombination processes are more important for slower ions with low z .

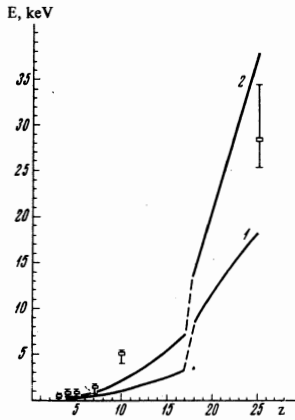


FIG. 10. Co_{59}^{17} ion energy as a function of ion charge. 1—Recombinational heating neglected, 2—strong recombinational heating.

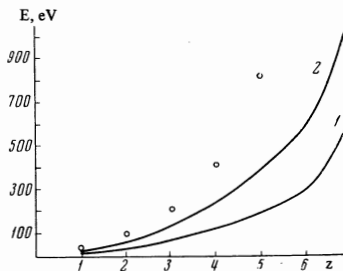


FIG. 11. Mn_{55}^{25} ion energy as a function of ion charge. 1—Recombinational heating neglected, 2—strong recombinational heating.

Effect of Recombination on the Ion Energy Spectra

Analysis of the energy spectra of ions corresponding to various elements, and the dependence of their shape on the laser intensity q , show that recombination processes play an important role in the formation of the energy spectrum.

The effect of recombination on the ion energy spectrum is particularly clearly seen in the series of measurements on Mn_{55}^{25} . Figure 6 shows the change in the ion distribution with increasing radiation intensity.

Let us consider the variation in the shape of the spectrum with increasing q . It is clear from Fig. 6a that, when $q = 2.5 \times 10^8 \text{ W-cm}^{-2}$, only singly-charged Mn ions are produced with energies of the order of 40 eV. Figure 6b corresponds to $q = 4.3 \times 10^8 \text{ W-cm}^{-2}$. Doubly charged ions with energies of about 150 eV appear at this intensity. At the same time, the singly-charged ion spectrum shows a peak roughly similar in shape to the doubly-ionized ion distribution. We assume that this peak is due to the recombination of doubly-charged ions into singly charged ions, and the energy of the resulting ions with $z = 1$ corresponds to the initial energy of ions with $z = 2$. Further increase in intensity results in the appearance of ions of higher charge. They provide a corresponding contribution to the energy distribution of ions with $z = 1$ and $z = 2$. If they succeed in recombining to any considerable extent, they affect only the distribution of ions with the preceding charge number. This is illustrated by the energy spectra of Figs. 6c, d, and e. When $q \sim 5.5 \times 10^8$ and 10^9 W-cm^{-2} , ions with $z = 3$ and $z = 4$ are not recorded, but the spectrum of ions with $z = 2$ affects their formation at the corresponding energy values. When $q \sim 2.5 \times 10^9 \text{ W-cm}^{-2}$, there are ions with $z = 3$ and $z = 4$, and the

spectrum corresponding to $z = 3$ has a peak in the energy region of $z = 4$ ions.

In general, the recombination of ions of charge z , which have high energies when they are produced, always contributes to the spectrum of ions with charges $(z - 1)$, $(z - 2)$, etc. in the high energy range.

Moreover, as a result of the increase in the kinetic energy with z , the fraction of ions having energy E greater than a certain value E^* will not succeed in recombining owing to their rapid emission. The result of this is that for ions with $z > z^*$ ($E^* = E(z^*)$) one observes a shift of the energy distributions relative to each other. Thus, the right-hand limits of the energy spectra for ions with high z correspond to the theoretical function $E = E(z)$ of Fig. 10, and in Fig. 4 it is clear that the shift of the curves begins for $z > z^* \approx 6-8$.

It is interesting to note that the angular distribution of the ions (Fig. 7) confirms the influence of recombination on the ion spectrum. Thus, it is clear from Fig. 7 that the angular distribution of ions with the same z but high energies tends to approach the normal to the target. This is connected with the fact that high-energy ions are formed as a result of the recombination of ions with high \bar{z} which have a highly elongated angular distribution lying near the normal (Fig. 7).

The energy distribution of ions is thus determined by recombination processes and, consequently, it can be used to deduce direct information about the recombination process.

CONCLUSION

We have shown that it is possible to produce highly charged ions which appear as a result of the "quenching" process. Our method has enabled us to investigate in detail the energy and the angular distributions, and it was noted that the energy of multiply charged ions was exceedingly high, up to 40 keV, and that they are emitted within a small solid angle. This substantially facilitates the extraction of the multiply-charged ion beam for practical purposes.

A detailed analysis was given above of the experimental data showing that the degree of ionization of the plasma ions can be estimated by the method put forward in^[11] and the well-known theory of interaction of laser radiation with matter^[3,4]. It turns out that it is possible to deduce information on the ionization potentials of multiply charged ions of various elements.

An interpretation was given above of the energy spectra of ions, which is based on the energy transfer between ions and electrons during emission of the plasma and their recombination (from z to $z - 1$). The role of recombination in the formation of the spectrum is additionally important because it can yield direct information on recombination processes involving high- z ions.

We are greatly indebted to N. G. Basov, O. N. Krokhin, and G. N. Flerov for their interest in this research and for useful discussions.

¹N. G. Basov, V. A. Boiko, V. A. Dement'ev, O. N. Krokhin, and G. V. Sklizkov, Zh. Eksp. Teor. Fiz. 51, 998 (1966) [Sov. Phys.-JETP 24, 659 (1967)].

²Yu. V. Afanas'ev, V. M. Krol', O. N. Krokhin, and I. V. Nemchinov, AMM 30, 1022 (1966).

³I. V. Nemchinov, PMM 31, 300 (1967).

⁴N. G. Basov, V. A. Gribkov, O. N. Krokhin, and G. V. Sklizkov, Zh. Eksp. Teor. Fiz. 54, 1073 (1968) [Sov. Phys.-JETP 27, 575 (1968)].

⁵P. Lunger, G. Tonon, F. Floux, and A. Ducaure, IEEE QE-2, 499 (1966); R. E. Elonig and J. R. Woolstone, Appl. Phys. Lett. 2, 139 (1963).

⁶Yu. A. Bykovskiĭ, V. I. Dorofeev, V. I. Dymovich, B. I. Nikolaev, S. V. Ryzhikh, and S. M. Sil'nov, Zh. Tekh. Fiz. 38, 1194 (1968) [Sov. Phys.-Tech. Phys. 13, 986 (1969)].

⁷Yu. A. Bykovskiĭ, N. N. Degtyarenko, V. I. Dymovich, V. F. Elesin, Yu. P. Kozyrev, B. I. Nikolaev, S. V. Ryzhikh, and S. M. Sil'nov, Zh. Tekh. Fiz. 39, 1694 (1969) [Sov. Phys.-Tech. Phys. 14, 1269 (1970)].

⁸V. V. Apollonov, Yu. A. Bykovskiĭ, N. N. Degtyarenko, V. F. Elesin, Yu. P. Kozyrev, and S. M. Sil'nov, ZhETF Pis. Red. 11, 377 (1970) [JETP Lett. 11, 252 (1970)].

⁹Yu. A. Bykovskiĭ, N. N. Degtyarenko, V. F. Elesin, Yu. P. Kozyrev, and S. M. Sil'nov, Izv. Vyssh. Ucheb. Zaved., Radiofiz. 13, 891 (1970).

¹⁰Yu. A. Bykovskiĭ, A. G. Dudoladov, N. N. Degtyarenko, V. F. Elesin, Yu. P. Kozyrev, and I. N. Nikolaev, Zh. Eksp. Teor. Fiz. 56, 1819 (1969) [Sov. Phys.-JETP 29, 977 (1969)].

¹¹Ya. B. Zel'dovich and Yu. P. Raĭzer, Fizika udra-nykh voln i vysokotemperaturnykh gidrodinamicheskikh yavleniĭ (Physics of Shock Waves and High-Temperature Hydrodynamic Phenomena), Nauka, 1966.

¹²A. V. Gurevich, L. V. Pariĭskaya, and L. P. Pitaevskiĭ, Zh. Eksp. Teor. Fiz. 49, 647 (1965) [Sov. Phys.-JETP 22, 449 (1966)].

¹³I. V. Nemtsov, Zh. Fiz. Khim. 29, 1031 (1955).

¹⁴Yu. V. Afanas'ev, É. M. Belenov, O. N. Krokhin, and I. A. Poluéktov, ZhETF Pis. Red. 10, 553 (1969) [JETP Lett. 10, 353 (1969)].

Translated by S. Chomet

143